Journal of Energy Storage 4 (2015) 121–127

Contents lists available at ScienceDirect

Journal of Energy Storage

journal homepage: www.elsevier.com/locate/est

Nano-porous activated carbon from sugarcane waste for supercapacitor application

Amrita Jain[a], S.K. Tripathi[b,*]

[a] School of Engineering and Information Technology, Manipal University, Dubai International Academic City, G-04, P.O. Box 345050, Dubai, United Arab Emirates

[b] Department of Physics, Jaypee University of Engineering and Technology, AB Road, Raghogarh 473226, Guna, Madhya Pradesh, India

ARTICLE INFO

Article history:
Received 26 July 2015
Received in revised form 19 September 2015
Accepted 30 September 2015
Available online 23 October 2015

Keywords:
Electrochemical double layer capacitors
Bagasse
Ionic liquid

ABSTRACT

Low cost with high specific capacitance and energy density is the critical and main requirement for practical supercapacitors. In the present work, nano porous activated carbon having specific surface area of 400 $m^2 g^{-1}$ from sugarcane waste (bagasse) has been synthesized and characterized as an electrode material for supercapacitor applications using ionic liquid based polymer gel electrolytes. The fabricated cell shows the overall specific capacitance of 372 mF cm^{-2} which is equivalent to single electrode specific capacitance of 248 F g^{-1}. The corresponding energy and power density of 16.3 Wh kg^{-1} and 1.66 kW kg^{-1} were achieved for EDLCs.

1. Introduction

Supercapacitors, also called as electrochemical capacitors or ultracapacitors are capable of providing large amount of energy in a short period of time, making them indispensable for fast power delivery [1–4]. In existing supercapacitors technologies most of the surface area resides in micropores that are not capable in forming electrical double layer; which results in the worst frequency response. Hence, energy stored in those carbon electrode materials can be withdrawn only at low frequencies. Nowadays, efforts have been focused on the development of supercapacitors having high energy and power density along with better frequency response for improved performance and more demanding applications [5–7].

Electrochemical double layer capacitors (EDLCs) have attracted a considerable attention due to their high power as well as energy density, excellent reversibility and long cycle life [8–9]. A wide range of carbonaceous materials like carbon aerogels [10], mesoporous carbons [11–12] and activated carbons [13–14], have been used as electrode materials in EDLCs.

Among these carbonaceous materials, biomass based activated carbon are most suitable because of its unique internal structure having regularly interconnected mesopores, high surface area, low mass density, notable chemical stability, acceptable electronic conductivity, low cost and environmental friendly nature makes it a promising electrode material for electrochemical double layer capacitors [2]. The large surface area of electrode is favorable for accumulating greater amount of charges leading to high energy density of the device. This ordered mesoporous structure enhances the diffusion rate of the charge carrier in the pore network which results in the better rate capability in high drain rate operations [15].

In the present manuscript, bagasse has been used as a biomass sample in order to prepare activated carbon. Chemical activation technique has been employed for the synthesis of bagasse based chemically treated activated charcoal (BCT) and has also been successfully checked as an electrode material for electrochemical double layer capacitor (EDLC) using ionic liquid as solid polymer electrolyte material. Ionic liquid based polymer gel electrolyte comprising of polyvinylidene fluoride hexafluoro propylene–1-ethyl-3-methylimidazolium bromide–propylene carbonate–Magnesium perchlorate, [PVdF(HFP)–(EMIM)(Br)–PC–$Mg(ClO_4)_2$] has been used because of its unique properties like low vapor pressure, high thermal stability and wide potential window [16]. The fabricated EDLC cell has been characterized by using a.c impedance, cyclic voltammetry and charge discharge techniques.

2. Experimental details

2.1. Preparation of ionic liquid based polymer electrolytes

The ionic liquid based polymer gel electrolytes using magnesium salts, [{polyvinylidene fluoride hexafluoro propylene}–{1-ethyl-3-methylimidazolium bromide}–{propylene carbonate}–{Magnesium perchlorate}] abbreviated as PVdF(HFP)–[EMIM]

* Corresponding author. Fax: +91 7544267011.
E-mail address: sktripathi16@yahoo.com (S.K. Tripathi).

http://dx.doi.org/10.1016/j.est.2015.09.010
2352-152X/

[Br]–PC–$Mg(ClO_4)_2$ has been prepared using standard "solution cast" techniques. In the process, initially the liquid electrolyte was optimized and prepared by dissolving 0.3 M magnesium salt in propylene carbonate (PC). The polymer PVdF-HFP and ionic liquid [EMIM][Br] was separately dissolved in acetonitrile. The liquid electrolyte was then mixed with the solution of PVdF-HFP/ [EMIM][Br]/acetonitrile in different weight ratios and stirred magnetically for 4–5 h. The concentration of PVdF-HFP and [EMIM][Br] was optimized and controlled at a ratio of 3:7. The viscous mixture was cast over glass petri dishes and acetonitrile was allowed to evaporate slowly, thereafter, free standing polymer gel electrolyte films (~400–450 μm) were obtained having ionic conductivity of $\sim 5.0 \times 10^{-3}$ S cm^{-1}. Finally the optimized polymer gel electrolyte of composition [PVdF(HFP) (30 wt%)–EMIM(Br) (70 wt%)] (30 wt%)–[PC–$Mg(ClO_4)_2$ (0.3 M)] (70 wt%) was used for the fabrication of supercapacitor cell.

2.2. Preparation of biomass charcoal and activated charcoal

Bagasse as a precursor material was obtained from the Guna district, Madhya Pradesh, India. Further it was cleaned from other materials such as sand or soil by washing it thoroughly. After that it was sun dried for 2–3 days. The dried bagasse was then kept in muffle furnace at 300 °C for 5 h. The charcoal was then soaked in chemical solution $CaCl_2$ (25 wt%) for 18–20 h and thereafter it was washed with double distilled water and kept in oven at 110 °C (overnight) for drying. Finally, chemical activation using KOH as an activating agent has been used for the synthesis of activated charcoal. The details of the procedure have been given elsewhere [17].

2.3. Construction of electrodes used in the experiments

The electrodes were prepared by making slurry of prepared activated charcoal powder and PVdF-HFP in the ratio 90:10 (w/w) in a common solvent acetone by thorough mixing. Fine films of electrodes were coated by spraying the slurry on carbon cloth (Ballard, USA) and kept in oven at 70 °C for 10–12 h by spraying the slurry on carbon cloth (Ballard, USA) and kept in oven at 70 °C for 10–12 h. The geometric surface area of electrode was taken as 1.0 cm^2 having 3.0 mg cm^{-2} as the mass of active electrode material.

2.4. Instrumental details

The pore texture characteristics and pore size distribution of the prepared activated charcoal was measured volumetrically with a Micrometrics Instruments, Gemini Model 2380 surface analyzer by N_2 desorption–adsorption technique using liquid N_2 at 77 K. The specific surface area was determined by using Brunauer–Emmett–Teller (BET) method in the pressure range (P/P_0) between 0.05 and 1.0. The pore size distribution (PSD) studies were carried out by using Barrett–Joyner–Halenda (BJH) method which was applied in the desorption branch of the isotherm. The sample was degassed at 300 °C for 2 h prior to adsorption experiments. X-ray diffraction studies have also been carried out by using D8 Advance, Bruker AXS Company, Germany using an operational voltage of 40 kV and current of 40 mA respectively by using CuKα radiation. A SEM-EDX image of the synthesized sample has been obtained by using FESEM, Zeiss, Ultra Plus 55. Thermogravimetric analysis (TGA) of the sample was performed after preheating it at 100 °C to remove adsorbed moisture and residual solvent. Then the mass loss was monitored in a thermogravimetric analyzer (TGA EXSTAR 6300).

2.5. Electrochemical measurements

Electrochemical measurements of the fabricated supercapacitor cells were carried out in a two-electrode cell. The cell has been fabricated as per the following configuration:

Cell A: BCT | [PVdF(HFP)−(EMIM)(Br)–PC–$Mg(ClO_4)_2$] | BCT

where BCT: bagasse based chemically treated activated charcoal and [PVdF(HFP)–(EMIM)(Br)–PC–$Mg(ClO_4)_2$] is optimized composition of polymer gel electrolyte used in the present studies and can be described as [{polyvinylidene fluoride hexafluoro propylene}–{1-ethyl-3-methylimidazolium bromide}–{propylene carbonate}–{magnesium perchlorate}].

The performance characteristics of the EDLC cell was carried out by using cyclic voltammetry, galvanostatic charge–discharge studies and a.c impedance spectroscopy with the help of computer controlled CHI 608C, CH Instruments, USA.

3. Results and discussion

3.1. Characterization of activated carbon

Activated carbons are high surface area and porous materials that are synthesized either by thermal or chemical activation method. It consists of small hexagonal rings called as graphene sheet. The size orientation and stacking of these sheets are determined by their synthesis method. During its activation process, the thermal energy involved is sufficient enough to break the links between adjacent graphene sheets which allows some of them to orient themselves in parallel. Fig. 1 shows the typical XRD pattern of BCT that consists of graphitic-like microcrystallites which are randomly oriented and distributed throughout the sample and confirms its turbostratic structure [18–20]. It can be clearly seen from the figure that there exists two broad diffraction peaks at 25° and 41.6° corresponding to (0 0 2) and (1 0 0) structural phases respectively which confirms the formation of activated charcoal.

In order to visualize the microstructure of the activated carbon, scanning electron microscopy (SEM) was performed and is shown in Fig. 2(a). Since the minor metallic impurities are generally associated with biomass based activated carbon therefore BCT has also been analyzed with energy dispersive X-ray spectroscopy (EDX) along with SEM and are shown in Fig. 2(b). EDX spectra reveal that the biomass based activated carbon contains minor quantities of silicon and oxygen. The presence of these elements is possibly due to the nature and history of biomass sample used (bagasse). The SEM image of BCT clearly shows the irregular and porous texture throughout the carbon surface, which facilitates the proper switching in and out of ions within the available pores and are mainly responsible for the better electrochemical performance of the devices.

Nitrogen adsorption–desorption isotherms of bagasse based activated carbon at 77 K are shown in Fig. 3. The isotherm is of type IV according to the IUPAC nomenclature [21] and it confirms the

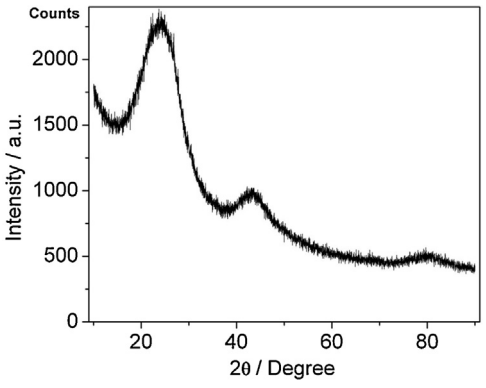

Fig. 1. XRD pattern of bagasse based activated charcoal.

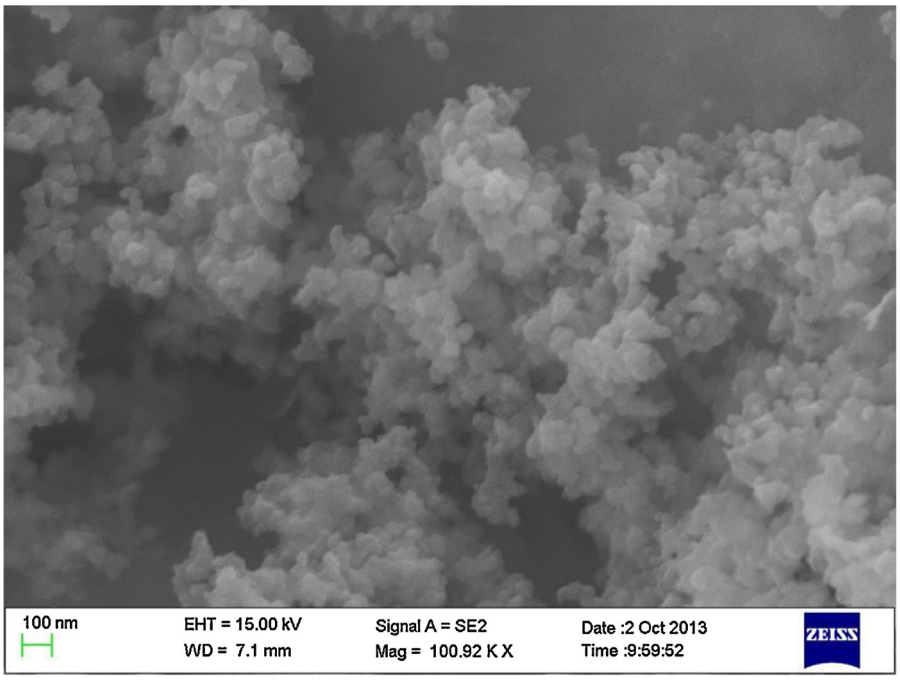

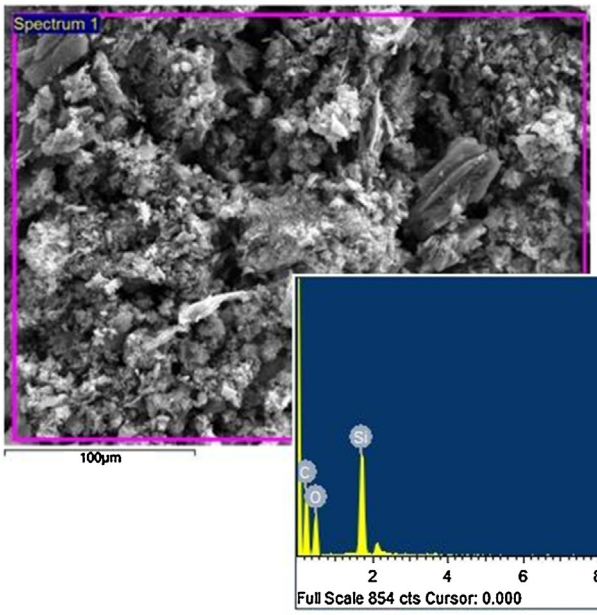

Element	Weight %	Atomic %
Carbon	55.23	65.93
Oxygen	29.08	26.06
Potassium	15.69	8.01

Fig. 2. SEM-EDX spectra of BCT electrode.

development of mesoporosity and microporosity of the prepared carbon which is desired from the supercapacitor application point of view. It can be seen from the isotherm that hysteresis loop can be observed at relatively high pressures ranging from 0.5 to 1.0 which clearly demonstrates the existence of substantial mesopores with larger pore size and can also be validated by its pore size distribution curve as shown in Fig. 3 (inset).

It can be seen that the adsorption uptake increases sharply at relative pressure ranging from 0.8 to 1.0 which confirms the formation of mesoporosity and macroporosity in the synthesized charcoal material. The electrochemical capacitance has a close correlation with the pore size distribution based on the theory of "double electric layer" energy storage mechanism [22,23]. Therefore in the present manuscript it has been observed that the pore size distributions lying between 2 and 5 nm have the most important contribution to the electrochemical characteristics of the BCT. It has been clearly seen from the inset of Fig. 3 that the value of micropore volume is appreciably high for bagasse based activated charcoal and it may be the main factor for its high specific capacitance values. The BET surface area, micropore volume and average pore diameter are enlisted in Table 1.

Fig. 4 shows the changes in weight as a function of temperature for chemically treated bagasse based activated charcoal. The entire temperature profile has been divided into three stages. The first stage occurs in the temperature range up to 150 °C and the weight loss at this stage is due to water release by evaporation and the sample has decomposed to non condensable gases like CO, CO_2, CH_4, H_2 etc [24]. In the second stage i.e. in between 200 °C and 600 °C, the weight loss observed is due to the thermal decomposition of raw materials, these reactions are accompanied by further

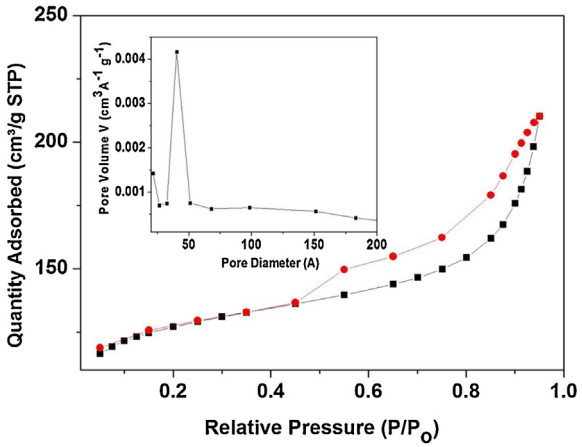

Fig. 3. Nitrogen adsorption–desorption isotherm and pore size distribution (inset) of BCT at 77 K.

Table 1
BET surface area, micropore volume and pore size of baggase based activated charcoal.

Sample	BET Surface area ($m^2\,g^{-1}$)	Micropore volume ($cm^3\,g^{-1}$)	Pore size (nm)
BCT[a]	400.0	0.101	4.0

[a]BCT = bagasse based chemically treated activated charcoal.

chemical transformations that include dehydration, degradation and condensation with a loss of aliphatic character which in turn increases the aromaticity and simultaneous release of gases [25]. The third stage shows the final weight loss which indicates that the active sites have reacted completely which is a measure of thermal stability of the synthesized material.

3.2. Electrochemical analysis

The electrochemical studies of EDLC cell were carried out by using electrochemical impedance spectroscopy, cyclic voltammetry and galvanostatic charge–discharge cycling.

Electrochemical impedance spectroscopy measurements were carried out by imposing a sinusoidal perturbation of 5.0 mV in the frequency range of 10 mHz–100 kHz. In the following section, a simple electrochemical impedance model has been discussed and the experimental results have been fitted with the theoretical model to determine different parameters associated with the EDLC cell under present investigations.

The typical a.c impedance plot of BCT based EDLC cell is shown in Fig. 5. A semicircle has been observed at higher frequency followed by a steep line in lower frequency region, which is a basic characteristic of supercapacitor cell.

As can be seen from the high frequency region of the plot that the diameter of semicircle is appreciably low, which is a measure of bulk resistance R_b and charge transfer resistance (R_{ct}) of the EDLC cell. Lower values of R_b and R_{ct} suggests the better performance of any electrochemical device, hence the EDLC cell in present studies shows excellent performance due to its lower values of resistance. Further, in the range of high-medium frequencies the impedance spectra clearly reflects a linear behavior with a slope of approximately 45° and below a certain frequency (particularly mHz in our case) the angle increases to almost 90°. This type of pattern is generally associated with the distribution of potential due to finite conductivities of the electrolyte materials within the compatible pores available in the electrode material [26]. The values of bulk resistance R_b and charge transfer resistance R_{ct} as calculated from the intercepts of real axis of the complex impedance response, along with the total resistance R and capacitance C measured at frequency of 10–100 mHz are summarized in Table 2.

In the present studies, hypothetical electrical circuit which consists of parameter with well defined electrical properties has been used to describe the impedance response of bagasse based EDLC cell. Fig. 6(a) gives the fitted impedance plot of the EDLC cell along with its simulation circuit. From the plot it can be seen that the fitted curve shows almost best fit in accordance with the experimental results having a minimum chi-squared value of 0.015 which has been calculated by using SAI ZPLOT Impedance analyzer software. Fig. 6(b) shows equivalent circuit model of the experimental results in which R_b is the bulk resistance, R_{ct} is the charge transfer resistance, C is the double layer capacitance, Z_W is the Warburg diffusion. In general, a capacitor circuit behaves as R–C transmission line circuit in the a.c response; therefore mostly impedance plot of supercapacitor cell consists of a semicircle in the high frequency and a linear part almost parallel to the imaginary axis in the lower frequency region. Those two regions are connected with a line of almost 45° slope and are referred to as Warburg impedance. In case of porous electrodes this is derived from ionic diffusion within the electrode material. Since the Warburg impedance is inversely proportional to the square root of

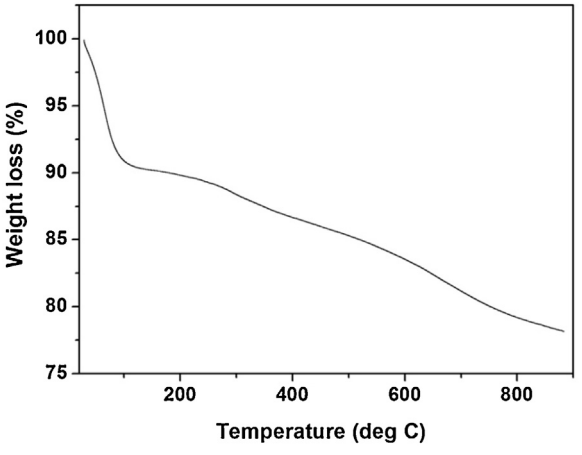

Fig. 4. Thermogravimetric curve (TGA) of BCT.

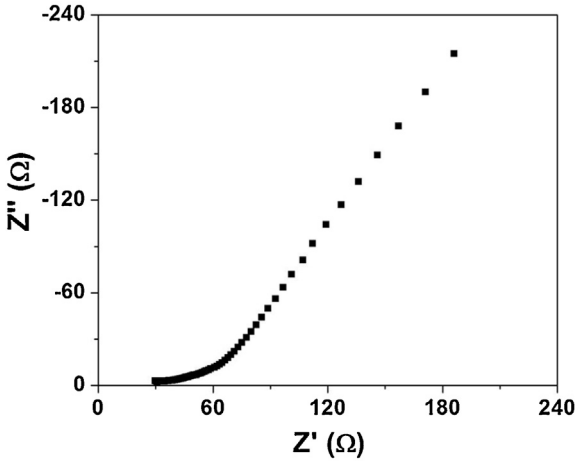

Fig. 5. AC impedance plot of an EDLC cell BCT | PVdF(HFP)–PC–$Mg(ClO_4)_2$–IL| BCT at room temperature.

Table 2
Electrical parameters of different EDLC cells from impedance analysis.

Cell	R_{ct} (Ω cm^2)	R_b (Ω cm^2)	100 mHz			10 mHz		
			R(Ω cm^2)	C		R(Ω cm^2)	C	
				(mF cm^{-2})[a]	(F g^{-1})[b]		(mF cm^{-2})[a]	(F g^{-1})[b]
A	5.8	6.0	20.3	58.4	38.9	56.7	372	248

[a] Overall capacitance of the cell.
[b] Single electrodes specific capacitance of the cell.

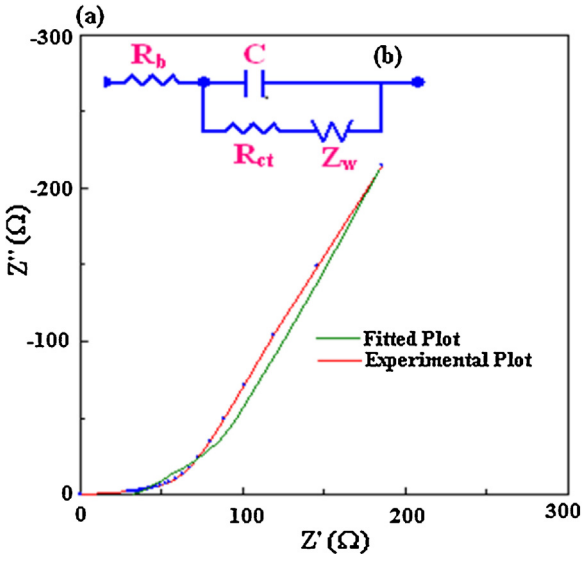

Fig. 6. (a) Experimental plot (red) and simulation plot (green) of the complex impedance spectrum of EDLC cell a (b) equivalent circuit model. (For interpretation of the reference to colour in this figure legend, the reader is referred to the web version of this article.)

frequency which suggests that it should be higher in the lower frequency region.

At high frequency, generally diameter of the semicircle represents diffusion of electrons within the electrode material (referred as charge transfer resistance, R_{ct}) and it depends on porosity of the electrodes, electrical conductivity of the material and effective accessible areas [30–31]. It can be clearly seen from the impedance plot that there is a depressed semicircular spur, which signifies that the electron transfer probably occurs within the large fraction of mesopores that allows easy accessibility of the charge transfer process. It is connected in-parallel in the equivalent circuit model (Fig. 6(b)). Further, the intercept on the real axis of the impedance plot shows the equivalent series resistance which is associated with the intrinsic resistance of the active carbon, the bulk resistance of the electrolyte and the contact resistance of the electrode. It is connected in-series in the equivalent circuit model. Further, on moving towards the right side of semicircle in equivalent circuit model, it includes the Warburg diffusion constant (Z_w) which represents the diffusion of ion into the bulk of electrode through pores of varying size.

The impedance frequency behavior was also studied by using complex model of the impedance [32–33]. The complex capacitance was calculated by using following equations:

$$C(\omega) = C'(\omega) - jC''(\omega) \tag{1}$$

where $C'(\omega)$ is the real part of complex capacitance $C(\omega)$. The lower frequency value of $C'(\omega)$ provides the capacitance value of EDLCs at lower scan/charge–discharge rate. $C''(\omega)$ is the imaginary part of the complex capacitance $C(\omega)$ and it gives an idea about the energy dissipation by an irreversible process that leads to a hysteresis. $C'(\omega)$ and $C''(\omega)$ are calculated by using the relations:

$$C'(\omega) = \frac{-Z''(\omega)}{\{\omega|Z(\omega)|^2\}} \tag{2}$$

$$C''(\omega) = \frac{Z'(\omega)}{\{\omega|Z(\omega)|^2\}} \tag{3}$$

where $Z'(\omega)$ and $Z''(\omega)$ are real and imaginary part of the complex impedance $Z(\omega)$ respectively and ω is the angular frequency which is given by $\omega = 2\pi f$.

Fig. 7(a) and (b) shows the variation of $C'(\omega)$ and $C''(\omega)$ with frequency. As can be seen from Fig. 7(a) that as frequency increases, the value of $C'(\omega)$ decreases and at high frequency the supercapacitor behaves like a pure resistor. The change of $C'(\omega)$ with frequency depends upon many factors like porous structure of electrode, electrode thickness and nature of electrolyte materials. The maximum point on the imaginary part of capacitance, as observed in the lower frequency region represents the complete system, which describes the transition point at which the circuit changes its behavior from purely resistive (higher frequency region) to purely capacitive character (lower frequency region) [34].

Complex power $S(\omega)$ of the fabricated cell was calculated by using the relation:

$$S(\omega) = P(\omega) + jQ(\omega) \tag{4}$$

where $P(\omega)$ is the real part of complex power, also known as active power and $Q(\omega)$ is the imaginary part of complex power, sometimes referred as reactive power. $P(\omega)$ and $Q(\omega)$ are evaluated by using the relation:

$$P(\omega) = \omega C''(\omega)|\Delta V_{rms}|^2 \tag{5}$$

$$Q(\omega) = -\omega C'(\omega)|\Delta V_{rms}|^2 \tag{6}$$

where $|\Delta V_{rms}|^2 = \frac{\Delta V_{max}}{\sqrt{2}}$ with V_{max} being the maximum amplitude of the a.c signal.

The plots of $|P|/|S|$ and $|Q|/|S|$ of the complex power vs. frequency (expressed in logarithmic scale) for EDLC cell is shown in Fig. 7(c) from where relaxation time constant τ_0 (=$2\pi f_0$) has been calculated which is the figure of merit of any supercapacitor cell. At high frequency when supercapacitor behaves like a pure resistor all the power is dissipated into the system (P = 100%), on the other hand at low frequency no power is dissipated into the system, where supercapacitor cells behave like a pure capacitor (P = 0%). The intersection of these two plot occurs at frequency f_0, which is also known as resonance frequency with the help of which relaxation time constant has been calculated. This time constant τ_0 belongs to the phase angle of 45° and it represents the behavioral change of supercapacitor from purely resistive to purely capacitive. It shows resistive behavior in the frequency $f > 1/\tau_0$ and capacitive for $f < 1/\tau_0$. In the present studies, the relaxation time constant is

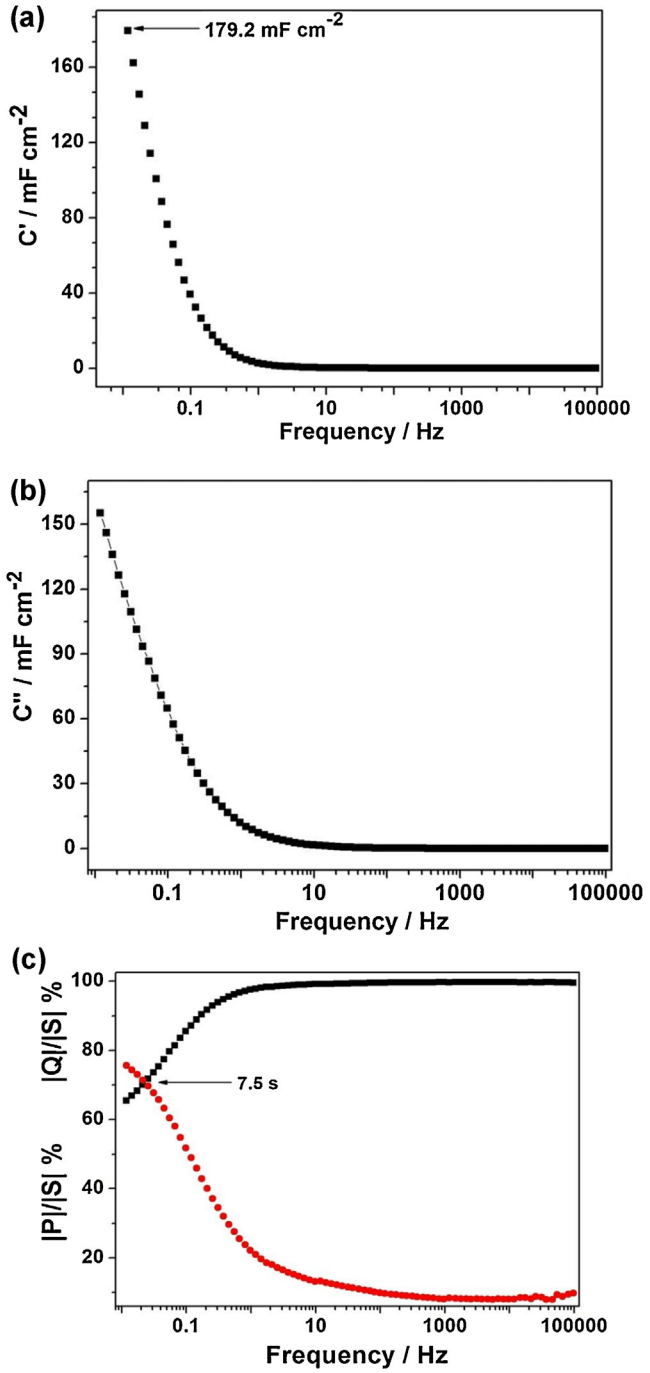

Fig. 7. Typical plots for the (a) real and (b) imaginary part of complex capacitance as a function of frequency (in logarithmic scale) for EDLC cell BCT | PVdF(HFP)–PC–$Mg(ClO_4)_2$–IL| BCT (c): normalized active power $|P|/|S|$ and reactive power $|Q|/|S|$ as a function of frequency (in logarithmic scale) for EDLC cell.

found to be 7.5 s which confirms the faster delivery of the stored charge which may be due to the lowering of ion transfer resistance and makes it a promising candidate for device application.

Cyclic voltammetry (CV) studies were also performed for bagasse based EDLC cell at different scan rates varying from 1.0 mV s^{-1} to 20 mV s^{-1} having upper and lower potential limits as $E_{sa} = 1.0$ V and $E_{sc} = -1.0$ V respectively. Cyclic voltammetry is an important tool that gives an idea about the capacitive behavior of the material used. It also helps us in finding out the various kind of information, like; nature of charge storage at interfaces in the

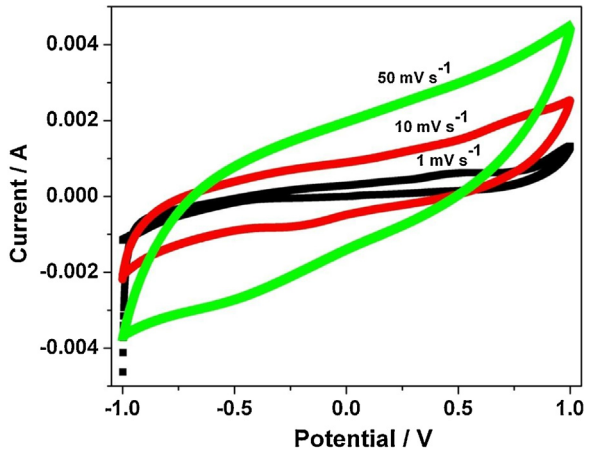

Fig. 8. Cyclic voltammograms of an EDLC cell BCT | PVdF(HFP)–PC–$Mg(ClO_4)_2$–IL| BCT at different scan rates.

anodic and cathodic region along with the overall behavior of the capacitor cell. Fig. 8 shows the cyclic voltammetry plot of the fabricated EDLC cell. It can be clearly seen from the plot that response of capacitor cell strongly depends on scan rate at which cyclic voltammogram has been carried out and it is the basic characteristics of real capacitor cell [35].

There is no evidence of redox current on both negative or positive voltammetric sweeps and current is almost constant over most of the potential range. With the increase in the scan rate, the CV curves tilted to some extent but still follows the rectangular shape which clearly shows that bagasse based electrodes has high power capability with ionic liquid based electrolytes [36–38]. The capacitance value from this technique is found to be 744 mF cm^{-2} which is equal to single electrode capacitance of 496 F g^{-1}.

In order to gain further understanding of the electrochemical properties of fabricated EDLCs, charge–discharge studies has also been carried out at constant current of 5.0 mA cm^{-2} and is shown in Fig. 9. It can be seen from the figure that curves are almost linear, which confirms its capacitive nature. In the beginning there is a sudden drop in the potential, it may be due to ohmic resistance associated with the device.

Hence it can be concluded that bagasse based electrodes are suitable for capacitive applications showing higher values of charge–discharge density. The specific capacitance, power and energy density values as obtained from charge–discharge curves are given in Table 3 [39].

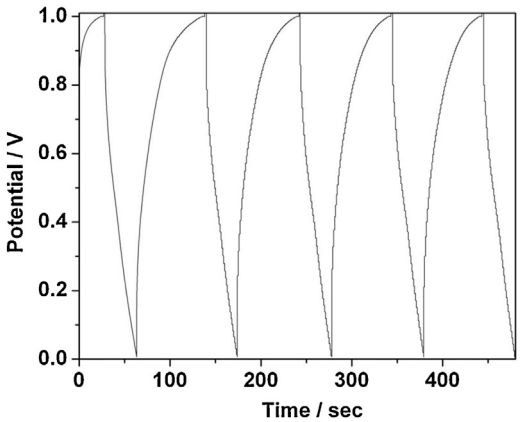

Fig. 9. Charge discharge curve of EDLC cell BCT | PVdF(HFP)–PC–$Mg(ClO_4)_2$–IL| BCT at a current density of 5.0 mA cm^{-2}.

Table 3
Typical charge–discharge characteristics of an EDLC cell at a current density of 5.0 mA cm^{-2}.

Cells	R_i ($\Omega\,cm^2$)	Discharge capacitance, C_d		Working voltage (V)	Energy density (Wh kg^{-1})	Power density (kW kg^{-1})
		(mF cm^{-2})[a]	(F g^{-1})[b]			
A	54.0	175.7	117.1	1.0	16.3	1.66

[a] Overall capacitance of the cell.
[b] Single electrodes specific capacitance of the cell.

4. Conclusion

High performance activated charcoal has been successfully prepared with low cost and waste bagasse. Chemical activation process has been used to synthesize the activated charcoal. The BET surface area for the prepared sample has been found to be 400 $m^2\,g^{-1}$. XRD studies and SEM-EDX spectra confirms that bagasse based activated carbon has well developed porosity and the main constituents of the prepared sample is predominantly graphite and amorphous carbon. Electrochemical studies clearly show the excellent capacitive behavior having specific capacitance of 372 mF cm^{-2} which is equivalent to single electrode capacitance of 248 F g^{-1}. The energy density of 16.3 Wh kg^{-1} and power density of 1.66 kW kg^{-1} has been achieved. Because of the unique characteristics, simple preparation and easy availability of material, bagasse can be considered as one of the potential material for supercapacitor application.

Acknowledgements

The authors are grateful to the Madhya Pradesh Council of Science and Technology, India for providing financial support through Grant-in-Aid for Scientific Research vide sanction no. [3683/CST/R&D/Phy & Engg. Sc/2012; Bhopal, Dated: 03.11.2012]. The authors are also thankful to Indian Institute of Technology, Roorkee, India for providing SEM-EDX, XRD and TGA results. We are also thankful to Dr. S.A. Hashmi, University of Delhi, India for providing BET data.

References

[1] R. Kötz, M. Carlen, Principles and applications of electrochemical capacitors, Electrochim. Acta 45 (2000) 2483–2498.
[2] B.E. Conway, Transition from supercapacitor to battery behavior in electrochemical energy storage, J. Electrochem. Soc. 138 (1991) 1539–1548.
[3] François Béguin, Elżbieta Frąckowiak, Supercapacitors: Materials, Systems and Applications, John Wiley and Sons, 2013.
[4] G.F. Gao, L.Y. Zhang, X.H. Chen, H. Jin, Preparation and characterization of peasecod-based activated carbons as electrode materials for electrochemical double-layer capacitors, Acta Phys. Chim. Sin. 27 (2011) 1679–1684.
[5] G.W. Yang, C.L. Xu, H.L. Li, Electrodeposited nickel foam with ultra high capacitance, Chem. Commun. 48 (2008) 6537–6539.
[6] Xiaojun He, Pinghua Ling, Jieshan Qiu, Moxin Yu, Xiaoyong Zhang, Chang Yu, Mingdong Zheng, Efficient preparation of biomass-based mesoporous carbons for supercapacitors with both high energy density and high power density, J. Power Sources 240 (2013) 109–113.
[7] M.M. Hantel, V. Presser, R. Kötz, Y. Gogotsi, In-situ electrochemical dilatometry of carbide derived carbons, Electrochem. Commun. 13 (2011) 1221–1224.
[8] J.R. Miller, P. Simon, Electrochemical capacitors for energy management, Science 321 (2008) 651–652.
[9] W. Li, H. Probstle, J. Fricke, J. Non-Cryst. Solids 325 (2003) 1–5.
[10] D.W. Wang, F. Li, M. Liu, et al., New Carbon Mater. 22 (2007) 307–314.
[11] F.Q. Zhang, Y. Meng, D. Gu, et al., Chem. Mater. 18 (2006) 5279–5288.
[12] D.W. Wang, F. Li, M. Liu, et al., Angew. Chem. Int. Ed. 47 (2008) 373–376.
[13] W. Xing, C.C. Huang, S.P. Zhuo, et al., Carbon 47 (2009) 1715–1722.
[14] Y.J. Kim, B.J. Lee, H. Suezaki, et al., Carbon 44 (2006) 1592–1595.
[15] C. Arbizzani, M. Biso, D. Cericola, et al., Safe, high-energy supercapacitors based on solvent-free ionic liquid electrolytes, J. Power Sources 185 (2) (2008) 1575–1579.
[16] M.A. Lillo-Rodenas, D. Cazorla-Amoros, A. Linares-Solano, Understanding chemical reactions between carbons and NaOH and KOH: an insight into the chemical activation mechanism, Carbon 41 (2003) 267–275.
[17] Amrita Jain, S.K. Tripathi, Ashish Gupta, Manju Mishra, Fabrication and characterization of electrochemical double layer capacitors using ionic liquid-based gel polymer electrolyte with chemically treated activated charcoal electrode, J. Solid State Electrochem. 17 (2013) 713–726.
[18] M. Awitdrus, I.A. Deraman, R. Talib, M.H. Omar, E. Jumali Taer, M.M. Saman, Sains Malaysiana 39 (2010) 83.
[19] A.R. Coutinho, J.D. Rocha, C.A. Luengo, Fuel Process. Technol. 67 (2000) 93.
[20] M. Deraman, S.K.M. Saat, M.M. Ishak, E. Awitdrus, I.A. Taer, R. Talib Omar, M.H. Jumali, AIP Proc. 1284 (2010) 179.
[21] K.S.W. Sing, D.H. Everett, R.A.W. Haul, L. Moscou, R.A. Pierotti, J. Rouquerol, T. Siemieniewska, Reporting physisorption data for gas solid systems with special reference to the determination of surface-area and porosity (Recommendations 1984), Pure Appl. Chem. 57 (1985) 603–619.
[22] P.Z. Guo, Q.Q. Ji, L.L. Zhang, S.Y. Zhao, X.S. Zhao, Preparation and characterization of peanut-shell-based microporous carbons as electrode materials for supercapacitors, Acta Phys. Chim. Sin. 27 (2011) 0001–0009.
[23] H.C. Liang, F. Chen, R.G. Li, L. Wang, Z.H. Deng, Electrochemical study of activated carbon semiconducting oxide composites as electrode materials of double-layer capacitors, Electrochim. Acta 49 (2004) 3463–3467.
[24] P. Fu, S. Hu, J. Xiang, L.S. Sun, S. Su, S.M. An, Study on the gas evolution and char structural change during pyrolysis of cotton stalk, J. Anal. Appl. Pyrolysis 97 (2012) 130–136.
[25] T.E. Rufford, D. Hulicova-Jurcakova, K. Khosla, Z.H. Zhu, G.Q. Lu, Microstructure and electrochemical double-layer capacitance of carbon electrodes prepared by zinc chloride activation of sugar cane bagasse, J. Power Sources 195 (2010) 912–918.
[26] R. de Levie, On porous electrodes in electrolyte solutions, Electrochim. Acta 8 (1963) 751–780.
[30] P. Justin, S.K. Meher, G.R. Rao, Tuning of capacitance behavior of NiO using anionic, cationic, and non ionic surfactants by hydrothermal synthesis, J. Phys. Chem. C 114 (2010) 5203–5210.
[31] K. Kierzek, E. Frackowiak, G. Lota, G. Gryglewicz, J. Machnikowski, Electrochemical capacitors based on highly porous carbons prepared by KOH activation, Electrochim. Acta 49 (2004) 515–523.
[32] V. Ganesh, S. Pitchumani, V. Lakshminarayanan, J. Power Soures 158 (2006) 1523.
[33] C. Portet, P.L. Taberna, P. Simon, E. Flahaut, J. Power Soures 139 (2005) 371.
[34] J. Wang, M. Chen, C. Wang, J. Wang, J. Zheng, J. Power Sources 196 (2011) 550–558.
[35] S. Jiali, C. hen, Y. hongyang, X. ang, L. ingwei, G. i, W. engchao, ang, High-performance asymmetric supercapacitor based on nanoarchitectured polyaniline/graphene/carbon nanotube and activated graphene electrodes, ACS Appl. Mater. Interfaces 5 (2013) 8467–8476.
[36] X. Zhou, L. Li, S. Dong, X. Chen, P. Han, H. Xu, J. Yao, C. Shang, Z. Liu, G. Cui, A renewable bamboo carbon/polyaniline composite for a high performance supercapacitor electrode material, J. Solid State Electrochem. 16 (2012) 877–882.
[37] W. Xiong, M. Liu, L. Gan, Y. Lv, Y. Li, L. Yang, Z. Xu, Z. Hao, H. Liu, L. Chen, A novel synthesis of mesoporous carbon microspheres for supercapacitor electrodes, J. Power Sources 196 (2011) 10461–10464.
[38] K. Kuratani, K. Okuno, T. Iwaki, M. Kato, N. Takeichi, T. Miyuki, T. Awazu, M. Majima, T. Sakai, Converting rice husk activated carbon into active material for capacitor using three-dimensional porous current collector, J. Power Sources 196 (2011) 10788–10790.
[39] F. Chaopeng, K. Yafei, H. Zhongyuan, W. Xiao, Y. Yifan, C. Jinhua, Z. Haihui, Supercapacitors based on graphene and ionic liquid electrolyte, J. Solid State Electrochem. 15 (2011) 2581–2585.